

Light cone tensor network and time evolution

Miguel Frías-Pérez^{1,2,*} and Mari Carmen Bañuls^{1,2}

¹Max-Planck-Institut für Quantenoptik, Hans-Kopfermann-Str. 1, D-85748 Garching, Germany

²Munich Center for Quantum Science and Technology (MCQST), Schellingstr. 4, D-80799 München

The transverse folding algorithm [Phys. Rev. Lett. 102, 240603] is a tensor network method to compute time-dependent local observables in out-of-equilibrium quantum spin chains that can sometimes overcome the limitations of matrix product states. We present a contraction strategy that makes use of the exact light cone structure of the tensor network representing the observables. The strategy can be combined with the hybrid truncation proposed for global quenches in [Phys. Rev. A 91, 032306], which significantly improves the efficiency of the method. We demonstrate the performance of this *transverse light cone contraction* also for transport coefficients, and discuss how it can be extended to other dynamical quantities.

INTRODUCTION

Tensor networks (TN) [1–3] have gained in the last decade a prominent role among numerical methods for quantum many-body systems. Simulating the dynamics of out of equilibrium systems remains nevertheless one of the most challenging open problems for these (and other) techniques.

In one dimensional systems, limitations of TN methods for dynamics are well understood: in global quenches the entanglement may grow fast [4–6], and the true state can escape the descriptive power of the TN ansatz. This so-called entanglement barrier limits the applicability of the matrix product state (MPS) [7–10] description, and makes it difficult to predict the asymptotic long-time behavior, even when local observables in this limit are expected to be well-described by a thermodynamic ensemble, itself well approximated by a matrix product operator (MPO) [11–16]. A number of methods have been suggested to try to overcome this issue and extract information about the long-time behavior of local properties [17–24]. While there is no universal solution, understanding the entanglement structures in the evolution TN can be crucial to identify the most adequate one for practical computations.

In particular, the transverse folding strategy [18, 25, 26] avoids the explicit representation of the evolved state as a MPS and instead focuses on contracting a TN that represents exactly (up to Trotter errors) the time-dependent observables. Instead of the standard evolution in time direction, the folding algorithm contracts the TN along space. In some scenarios, this allows local observables to be computed to longer times than other approaches [27], and it is an exact strategy for certain models [28]. Recently, there has been a rekindled interest in this approach, triggered by the interpretation of the network in terms of an influence functional [29–31].

In local lattice models, the velocity of propagation of information is upper-bounded [32–34] and the exact TN for observables has a light cone structure. While there have been proposals that exploit this fact to reduce the

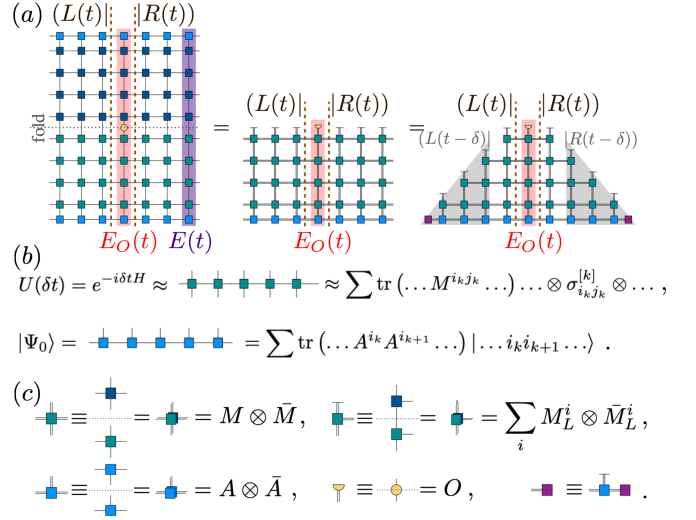


FIG. 1. (a, b) Schematic construction of the minimal TN for the expectation value of a local operator O after a global quench in a translationally invariant setting. At time $t = M\delta$ the expectation value $\langle \Psi(t) | O | \Psi(t) \rangle$ corresponds to a two dimensional TN. After folding, the exact light cone is obtained after removing the mutually cancelling gates. (c) Graphical notation for folded TN diagrams through the paper.

cost of the numerical simulation of the evolved state with TN [35–37], and with quantum simulation [38], until now, the potential of combining it with the transverse strategy has not been explored.

Here we propose a strategy to exploit this property, a *transverse light cone contraction* of the TN (TLCC). This improves the efficiency by reducing the computational effort to that of approximating the minimal network describing the time-dependent observables in a Trotterized evolution. We demonstrate explicitly its performance for global quenches and different-time thermal correlators at infinite temperature, and investigate how the strategy can make use of the (more efficient) physical light cone determined by the Lieb-Robinson velocity [33]. We discuss possible extensions to other interesting quantities.

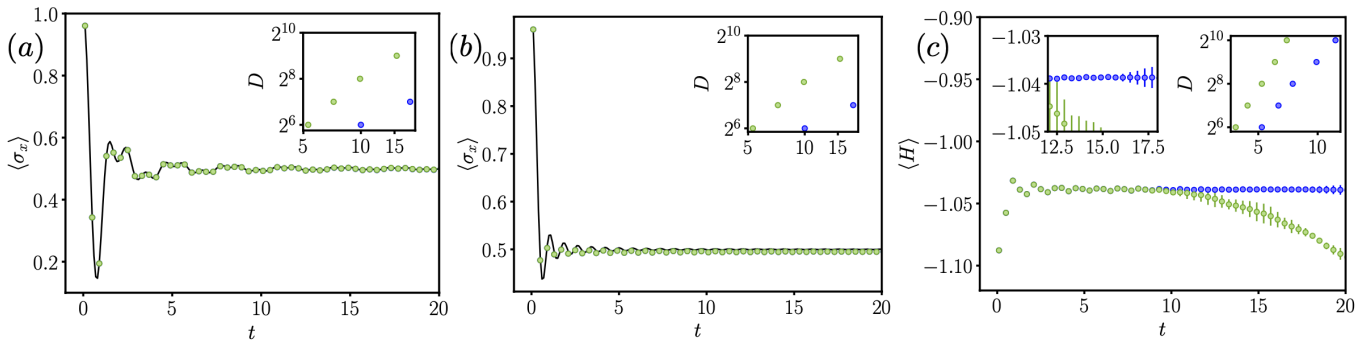


FIG. 2. Global quenches, from the initial state $|X+\rangle$, for the integrable [(a) $g = 0.5$, (b) $g = 1$] and non-integrable [(c) $g = -1.05$, $h = 0.5$] Ising model. The main plots show the transverse magnetization $\langle \sigma_x(t) \rangle$ (a, b) for bond dimension $D = 128$, and the energy density (c) for bond dimension $D = 512$. Error bars represent the difference with respect to a smaller bond dimension, $D' = 64$ for (a, b) and $D' = 256$ for (c). Truncations of the boundary vectors were performed with a standard MPS algorithm (green) and with the hybrid algorithm of [26] (blue). The insets show the scaling of the bond dimension required to keep constant precision in each algorithm. In the integrable case, this is compatible (at the later times) with a polynomial increase $D \sim t^\alpha$, consistent with observations in [25, 39]. In the non-integrable case, the increase is compatible with an exponential growth for both truncation methods, but using the hybrid truncation exhibits a slower rate than standard ones, such that longer times can be reached with the same bond dimension. The left inset in (c) shows a zoom of the main plot to better appreciate the differences.

LIGHT CONE TENSOR NETWORK FOR GLOBAL QUENCHES

The one-dimensional global quench is a natural test bench for time-evolution TN algorithms. At time $t = 0$ the system is prepared in a state that can be written as a MPS (e.g. a product state), and then it is let to evolve under a fixed Hamiltonian. For simplicity, we restrict the discussion to a nearest-neighbour model, and a translationally invariant case, but the construction generalizes straightforwardly to any model with local (finite-range) interactions and some non-translationally invariant scenarios.

The transverse folding proposal of [18] starts from a two-dimensional TN whose contraction represents some time-dependent observable, such as a local expectation value. This TN can be constructed from a Suzuki-Trotter approximation of the evolution operator, where the evolution for a discrete step of time δ can be approximated as a matrix product operator (MPO) [11, 12] with a small bond dimension, constructed from a product of two-body gates [13]. The TN for the observable at time $t = M\delta$ is obtained by applying M copies of this MPO with the initial state, which yields the evolved state, and contracting the operator of interest between this and its adjoint.

While standard TN algorithms as TEBD or tMPS [11, 40–42] compute the observable by contracting the network in the time direction, the transverse folding strategy performs the contraction in the spatial direction, after folding the TN in half, such that tensors for the same site and time step in the ket and the bra are grouped together (see figure 1a). This can result in a reduction of the entanglement along the time direction, which often allows reaching longer times than standard algo-

gorithms [25]. For a translationally invariant system in the thermodynamic limit, such contraction reduces to an expectation value of the form $\langle L(t)|E_O(t)|R(t) \rangle$, where $\langle L(t)|$ and $|R(t)\rangle$ are the dominant left and right eigenvectors of the transfer operator $E(t) = \sum_i A^i(t) \otimes A^i(t)$, and $E_O(t) = \sum_i A^i(t) \otimes A^j(t) \langle i|O|j \rangle$ [10]. Here, $A^i(t)$ represents the *concatenated* [43] local tensor of the time-dependent state, itself a MPO. In the transverse folding strategy, the boundary vectors $\langle L(t)|$ and $|R(t)\rangle$ are approximated by MPS. This approximation can be found, for instance, via a power iteration or a Lanczos algorithm, using repeated MPO-MPS contractions.

Such strategies do not take into account that the TN has a light cone structure. Because the individual gates are local, outside the causal cone of the operator, each gate cancels with its adjoint. This ensures that each of the required boundary vectors (dominant eigenvectors of the transfer operator) corresponds precisely to the contraction of a triangular network as depicted in fig. 1. We can approximate directly the contraction of such triangle in the space direction by a MPS. This strategy, which we call *transverse light cone contraction* (TLCC), allows us to obtain $\langle L(t)|$ and $|R(t)\rangle$ in a fixed number of steps (proportional to M). Furthermore, once we have found the vectors for M time steps, we can directly obtain them for $M + 1$ by applying a single MPO (as illustrated in the figure), which increases the length by one, and approximating the result via a single truncation step. This step can be performed using standard MPS truncation algorithms, which reduce the bond dimension by minimizing a distance between the truncated vector and the original one. However, for this particular problem the *hybrid* truncation algorithm proposed in [26], which effectively

evolves the bond of the boundary vector according to the real time dynamics, yields a much more efficient use of the available bond dimension (see also insets of fig. 2).

The TLCC strategy results in a more efficient algorithm than the originally proposed folding, which required iterative MPO-MPS contractions until convergence of the dominant eigenvectors, run independently for each different time step. Notice, nevertheless, that if the bond dimension used is large enough, both the original folding algorithm and the TLCC should result in the same boundary vector. What ultimately determines the applicability of transverse strategies is thus the amount of *entanglement* present in the transverse network.

To probe the performance of the method, we consider a quantum Ising chain, initialized in a product state $|X+\rangle = \lim_{N \rightarrow \infty} [(|0\rangle + |1\rangle)/\sqrt{2}]^{\otimes N}$. We then apply the Hamiltonian,

$$H_I = \sum_i (J\sigma_i^z \sigma_{i+1}^z + g\sigma_i^x + h\sigma_i^z), \quad (1)$$

and compute local expectation values after time evolution. In all the following we fix $J = 1$, and a Trotter step $\delta = 0.1$, and vary the parameters of the model to study integrable ($g = \{0.5, 1\}$, $h = 0$) and non-integrable ($g = -1.05$, $h = 0.5$) regimes. Figure 2 shows the results and demonstrates that the TLCC can efficiently simulate the integrable quenches. In the non-integrable regime, the required bond dimension grows much faster with time, but the method is still advantageous as compared to standard evolution, much more so when the truncation is performed as in [26] (see inset of fig. 2c).

LIGHT CONE TENSOR NETWORK FOR TRANSPORT COEFFICIENTS

The same idea can be adapted to the computation of other dynamical quantities. It is the case of thermal correlators, of the form $C_{1,2}(t, \ell, \beta) = \text{tr}(\rho_\beta O_2^{[\ell]}(t) O_1^{[0]}(0))$, where $\rho_\beta = e^{-\beta H}/Z$ is the thermal equilibrium state at inverse temperature β , $Z = \text{tr}(e^{-\beta H})$ is the partition function, $O_k^{[\ell]}(t)$ is a (local) operator acting on site ℓ at time t , and $O_k(t) = U(t)^\dagger O_k U(t)$ is the time-evolved operator in Heisenberg picture. Since $[\rho_\beta, H] = 0$, the thermal state is invariant under the evolution, and using $\rho_\beta \propto \rho_{\beta/2} \rho_{\beta/2}^\dagger$ we can write (up to normalization), $C_{1,2}(t, \ell, \beta) \propto \text{tr}(U(t)^\dagger \rho_{\beta/2}^\dagger O_2^{[\ell]} U(t) O_1^{[0]} \rho_{\beta/2})$. Using a MPO approximation to $\rho_{\beta/2}$ (obtained with standard TN methods [11, 12, 44]), and the Trotterized evolution as in the previous section, this quantity can be expressed as a two dimensional folded TN, which can be contracted in the temporal [45] or spatial (transverse) [25] direction.

Due to the invariance of the thermal state, each local observable generates also a light cone structure that can

be exploited in the TLCC approach. Now the cancellation of gates outside the causal cone of the operators occurs both at the upper and the lower parts of the network (see figure 3a), and the minimal TN has a rectangular form, resembling a pillow, a structure which was used in [46] to evaluate correlators in random quantum circuits. The TLCC strategy again requires contracting a triangular TN corresponding to the lateral corners of the figure to obtain boundary vectors $|L_\beta(t)\rangle$ and $|R_\beta(t)\rangle$. [47] If both operators act on the same site ($\ell = 0$), the time dependent correlators can be expressed as a contraction $\langle L_\beta(t) | T_{\beta, O_1, O_2}(t) | R_\beta(t) \rangle$, with a single MPO $T_{\beta, O_1, O_2}(t)$ constructed from concatenating the local tensors for the unitaries, the operators and the states (see fig. 3a). For correlators at non-zero distance ℓ the minimal TN becomes elongated (fig. 3a, lower diagrams). To approximate its contraction, the boundary vectors $|L_\beta(t)\rangle$ and $|R_\beta(t)\rangle$ for a certain time t are first grown to incorporate, respectively, O_1 at the bottom of the TN, and O_2 at the top. These extended vectors contain the evolution steps up to time $t + 2\delta$, and can be contracted together to obtain the correlators at $\ell = 1$ for times $t + 3\delta$ and $t + 4\delta$. The vectors can be then evolved again, following the TN structure, which does not increase their length, but allows access to correlators at any later time $t + (2+k)\delta$ and distances $\ell = k, k+1$. Applying this systematically we can obtain all non-vanishing correlators. This generalizes trivially to operators on more than one site, or with MPO structure.

Here we illustrate the simplest case, infinite temperature, where $\rho_{\beta=0} \propto \mathbb{1}$ and the contour of the TN becomes uncorrelated. We consider the energy density operator

$$O_E^{[i]} := J\sigma_i^z \sigma_{i+1}^z + \frac{g}{2}(\sigma_i^x + \sigma_{i+1}^x) + \frac{h}{2}(\sigma_i^z + \sigma_{i+1}^z), \quad (2)$$

which can be written as a MPO of range 2. Figure 3b shows our results for the correlators $C_{EE}(t, \ell, \beta = 0)$ as a function of time for several distances in the non-integrable ($g = -1.05$, $h = 0.5$, main plot) and integrable ($g = 0.5$, $h = 0$, inset) cases.

Specially interesting is the possibility of ab initio calculations of transport properties [48] in non-integrable models. In particular, diffusion constants can be related to the spatial spreading in time of autocorrelations of a density [20, 49, 50]. Normalizing the correlators as $\tilde{C}_{EE}(0, \ell) := C_{EE}(t, \ell) / \sum_\ell C_{EE}(0, \ell)$, a diffusion constant $\mathcal{D}(t)$ may be obtained from their spatial variance [49]

$$W^2(t) := \sum_\ell \tilde{C}_{EE}(t, \ell) \ell^2 - \left(\sum_\ell \tilde{C}_{EE}(t, \ell) \ell \right)^2, \quad (3)$$

as $\frac{\partial W^2}{\partial t} = 2\mathcal{D}(t)$. Figure 3c shows the (linearly growing) variance $W^2(t)$ (main plot), and the corresponding diffusion constant (inset) obtained from the correlators for the

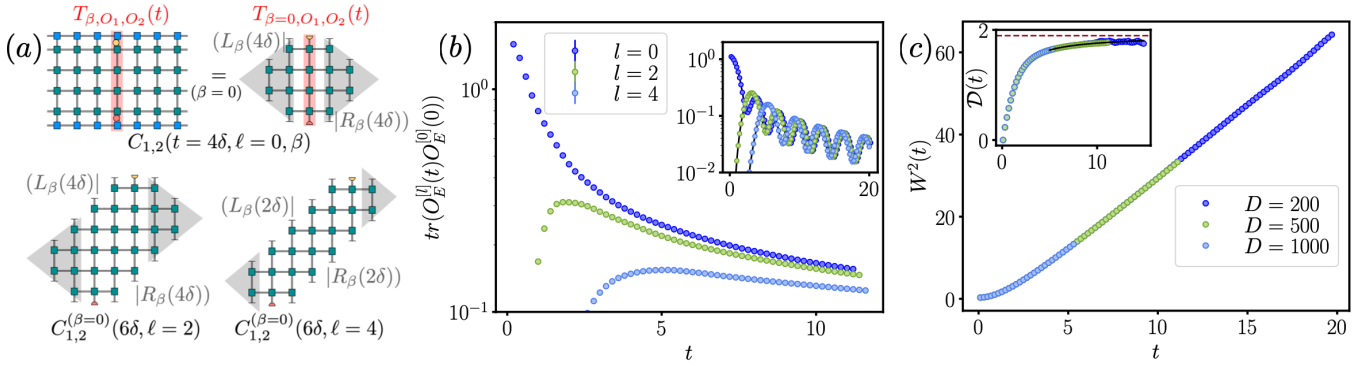


FIG. 3. (a) Schematic construction of the minimal TN for two-point correlators at infinite temperature for different times and distances. (b) Energy autocorrelations $C_{EE}(t, \ell, \beta = 0)$ at several distances as a function of time in the integrable ($g = 0.5$, inset) and non-integrable ($g = -1.05, h = 0.5$, main plot) Ising chain at $\beta = 0$. The error bars (smaller than the size of the marker) show the difference between results with two different bond dimensions (D, D') [for the inset (200, 100), for main plot (500, 200)]. (c) Spatial variance 3 of the normalized autocorrelations (main plot) and corresponding diffusion constant (inset) in the non-integrable case. The solid black line in the inset shows a fit of the form $\mathcal{D}_E \exp(b/t)$, which predicts the asymptotic value $\mathcal{D}_E \approx 1.9$ (red dotted line).

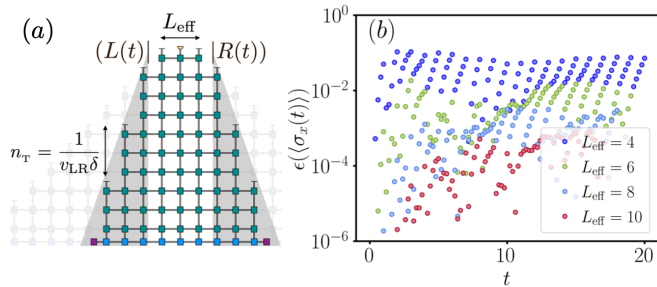


FIG. 4. (a) The physical velocity defines a much narrower light cone than the Trotterization (background). (b) Relative difference between $\langle \sigma_x \rangle$ computed with the LR and Trotter light cones for the integrable global quench of fig. 2a, for which $n_T = 10$ and different sizes of the subsystem L_{eff} , with $D = 200$ in all cases.

non-integrable case. The diffusion constant is well fitted by a function $\mathcal{D}(t) = \mathcal{D}_E \exp(b/t)$, compatible with saturation to a constant $\mathcal{D}_E \approx 1.9$ in the asymptotic regime.

THE PHYSICAL LIGHT CONE

In general, we expect that the physical light cone is much narrower than the trivial one from the Trotterization, used in the previous sections. We could thus approximate the TN by a light cone one in which the slope corresponds to the maximal physical velocity v_{LR} . This can be achieved by implementing a more efficient TLCC growing iteration, in which $n_T = 1/(v_{\text{LR}}\delta)$ time steps are applied at once every time a space site is contracted (fig. 4a). Notice that this light cone is not exact, but has (exponential) corrections. Thus it is convenient to consider the light cone for a subsystem of size L_{eff} that

includes the support of the operator.[51]

To probe this reduced light cone we choose an integrable instance, ($g = 0.5, h = 0$), for which the Lieb-Robinson velocity is known ($v_{\text{LR}} = 1$, corresponding to $n_T = 10$ with our Trotter step), and simulate the global quench of fig. 2a. Compared to TLCC for the full light cone with the same bond dimension, we observe (fig. 4) that the physical one, determined by v_{LR} , captures indeed the correct evolution: while the narrower light cone deviates from full results, the errors are reduced exponentially (until the level of original truncation error) by considering a small window L_{eff} .

DISCUSSION

We have presented a strategy that builds on the transverse folding [18] to approximate time-dependent observables in a one-dimensional quantum system. Noticing the exact light cone structure of the TN and implementing its transverse contraction, it is possible to compute long time properties in a more efficient manner. Combined with the hybrid truncation [26], this allows us, in certain scenarios, to reach longer times with a smaller bond dimension. It is possible to use the physical upper bound of the Lieb-Robinson velocity to further restrict the width of the relevant TN and define a more efficient iteration.

We have evaluated the performance of the TLCC strategy for integrable and non-integrable global quenches, and for transport properties at infinite temperature. With minimal changes, the method extends to other scenarios, such as finite temperature or non translationally invariant setups including impurities or a contact between two chains. It is furthermore possible to adapt the strategy to other more complex dynamical quantities.

The basic TLCC does not require additional hypothesis to truncate observables or states. Its convergence can be systematically explored as the bond dimension is increased. What ultimately limits the validity of the strategy is the entanglement in the time direction, which strongly depends on the setup and the model [25, 39, 52]. The behavior of the TLCC can thus provide useful information to determine optimal strategies for different problems. Another parameter in the approximation is the Trotter step, which is known to affect the entanglement growth in standard algorithms [42]. Since simulations with different δ may be necessary to extrapolate the exact results, it is also interesting to study how varying δ affects our observations. Further interesting avenues for future investigation are exploring the TN cut according to different velocities, to explore the propagation of correlations in the TN and effectively measure v_{LR} .

While we were completing this manuscript, an equivalent strategy for global quenches was independently suggested in [53].

We are thankful to J. I. Cirac, M. Hastings and L. Tagliacozzo for insightful discussions at different stages of this project. This work was partly supported by the Deutsche Forschungsgemeinschaft (DFG, German Research Foundation) under Germany's Excellence Strategy – EXC-2111 – 390814868. M.C.B. acknowledges the hospitality of KITP, where earlier versions of the work were developed, with support from the National Science Foundation under Grant No. NSF PHY-1748958.

* miguel.frias@mpq.mpg.de

- [1] F. Verstraete, V. Murg, and J. Cirac, *Adv. Phys.* **57**, 143 (2008).
- [2] U. Schollwöck, *Ann. Phys.* **326**, 96 (2011).
- [3] R. Orús, *Ann. Phys.* **349**, 117 (2014).
- [4] P. Calabrese and J. Cardy, *Journal of Statistical Mechanics: Theory and Experiment* **2005**, P04010 (2005).
- [5] T. J. Osborne, *Phys. Rev. Lett.* **97**, 157202 (2006).
- [6] N. Schuch, M. M. Wolf, F. Verstraete, and J. I. Cirac, *Phys. Rev. Lett.* **100**, 030504 (2008).
- [7] M. Fannes, B. Nachtergaele, and R. F. Werner, *Communications in Mathematical Physics* **144**, 443 (1992).
- [8] G. Vidal, *Phys. Rev. Lett.* **91**, 147902 (2003).
- [9] F. Verstraete, D. Porras, and J. I. Cirac, *Phys. Rev. Lett.* **93**, 227205 (2004).
- [10] D. Pérez-García, F. Verstraete, M. M. Wolf, and J. I. Cirac, *Quantum Inf. Comput.* **7**, 401 (2007).
- [11] F. Verstraete, J. J. García-Ripoll, and J. I. Cirac, *Phys. Rev. Lett.* **93**, 207204 (2004).
- [12] M. Zwolak and G. Vidal, *Phys. Rev. Lett.* **93**, 207205 (2004).
- [13] B. Pirvu, V. Murg, J. I. Cirac, and F. Verstraete, *New J. Phys.* **12**, 025012 (2010).
- [14] M. B. Hastings, *Phys. Rev. B* **73**, 085115 (2006).
- [15] A. Molnar, N. Schuch, F. Verstraete, and J. I. Cirac, *Phys. Rev. B* **91**, 045138 (2015).
- [16] T. Kuwahara, A. M. Alhambra, and A. Anshu, *Phys. Rev. X* **11**, 011047 (2021).
- [17] M. J. Hartmann, J. Prior, S. R. Clark, and M. B. Plenio, *Phys. Rev. Lett.* **102**, 057202 (2009).
- [18] M. C. Bañuls, M. B. Hastings, F. Verstraete, and J. I. Cirac, *Phys. Rev. Lett.* **102**, 240603 (2009).
- [19] C. D. White, M. Zaletel, R. S. K. Mong, and G. Refael, *Phys. Rev. B* **97**, 035127 (2018).
- [20] T. Rakovszky, C. W. von Keyserlingk, and F. Pollmann, “Dissipation-assisted operator evolution method for capturing hydrodynamic transport,” (2020), arXiv:2004.05177.
- [21] C. Krumnow, J. Eisert, and Ö. Legeza, “Towards overcoming the entanglement barrier when simulating long-time evolution,” (2019), arXiv:1904.11999.
- [22] J. Surace, M. Piani, and L. Tagliacozzo, *Phys. Rev. B* **99**, 235115 (2019).
- [23] M. M. Rams and M. Zwolak, *Phys. Rev. Lett.* **124**, 137701 (2020).
- [24] J. Lopez-Piqueres, B. Ware, S. Gopalakrishnan, and R. Vasseur, *Phys. Rev. B* **104**, 104307 (2021).
- [25] A. Müller-Hermes, J. I. Cirac, and M. C. Bañuls, *New Journal of Physics* **14**, 075003 (2012).
- [26] M. B. Hastings and R. Mahajan, *Phys. Rev. A* **91**, 032306 (2015).
- [27] M. C. Bañuls, J. I. Cirac, and M. B. Hastings, *Phys. Rev. Lett.* **106**, 050405 (2011).
- [28] L. Piroli, B. Bertini, J. I. Cirac, and T. c. v. Prosen, *Phys. Rev. B* **101**, 094304 (2020).
- [29] M. Sonner, A. Leroise, and D. A. Abanin, *Annals of Physics* **435**, 168677 (2021).
- [30] A. Leroise, M. Sonner, and D. A. Abanin, *Phys. Rev. X* **11**, 021040 (2021).
- [31] E. Ye and G. K.-L. Chan, *The Journal of Chemical Physics* **155**, 044104 (2021).
- [32] E. H. Lieb and D. W. Robinson, *Communications in Mathematical Physics* **28**, 251 (1972).
- [33] M. B. Hastings and T. Koma, *Communications in Mathematical Physics* **265**, 781 (2006).
- [34] B. Nachtergaele and R. Sims, *Communications in Mathematical Physics* **265**, 119 (2006).
- [35] M. B. Hastings, *Journal of Mathematical Physics* **50**, 095207 (2009).
- [36] T. Enss and J. Sirker, *New Journal of Physics* **14**, 023008 (2012).
- [37] E. Gillman, F. Carollo, and I. Lesanovsky, *Phys. Rev. A* **103**, L040201 (2021).
- [38] J. Haah, M. B. Hastings, R. Kothari, and G. H. Low, *SIAM Journal on Computing* **SPECIAL SECTION FOCS 2018**, FOCS18 (2018).
- [39] G. Giudice, G. Giudici, M. Sonner, J. Thoenness, A. Leroise, D. A. Abanin, and L. Piroli, “Temporal entanglement, quasiparticles and the role of interactions,” (2021), arXiv:2112.14264 [cond-mat.stat-mech].
- [40] G. Vidal, *Phys. Rev. Lett.* **93**, 040502 (2004).
- [41] G. Vidal, *Phys. Rev. Lett.* **98**, 070201 (2007).
- [42] S. Paeckel, T. Köhler, A. Swoboda, S. R. Manmana, U. Schollwöck, and C. Hubig, *Annals of Physics* **411**, 167998 (2019).
- [43] R. Hübener, V. Nebendahl, and W. Dür, *New Journal of Physics* **12**, 025004 (2010).
- [44] A. E. Feiguin and S. R. White, *Phys. Rev. B* **72**, 220401 (2005).
- [45] T. Barthel, *New Journal of Physics* **15**, 073010 (2013).

- [46] C. Sünderhauf, D. Pérez-García, D. A. Huse, N. Schuch, and J. I. Cirac, Phys. Rev. B **98**, 134204 (2018).
- [47] Different from the global quench above, in this case each iteration of the algorithm grows the boundary vectors in two time steps.
- [48] B. Bertini, F. Heidrich-Meisner, C. Karrasch, T. Prosen, R. Steinigeweg, and M. Žnidarič, Rev. Mod. Phys. **93**, 025003 (2021).
- [49] R. Steinigeweg, H. Wichterich, and J. Gemmer, EPL (Europhysics Letters) **88**, 10004 (2009).
- [50] H. Kim and D. A. Huse, Phys. Rev. Lett. **111**, 127205 (2013).
- [51] Equivalently, we can *insert* in the middle of the column, corresponding to an earlier time.
- [52] A. Leroose, M. Sonner, and D. A. Abanin, Phys. Rev. B **104**, 035137 (2021).
- [53] A. Leroose, M. Sonner, and D. A. Abanin, “Overcoming the entanglement barrier in quantum many-body dynamics via space-time duality,” (2022), arXiv:2201.04150 [quant-ph].